MALAYSIAN JOURNAL OF ANALYTICAL SCIENCES

Journal homepage: https://mjas.analis.com.my/

Research Article

Unveiling the inhibitory mechanisms of ribavirin, EGCG and ST-610 on NS3 helicase of DENV2 through docking and molecular dynamics simulations

Aina Hazimah Bahaman[1], Bimo Ario Tejo[1,2], Siti Munirah Mohd Faudzi[1,3] and Mohd Basyaruddin Abdul Rahman[1]*

[1] Department of Chemistry, Faculty of Science, Universiti Putra Malaysia, 43400 UPM Serdang, Selangor Darul Ehsan, Malaysia
[2] Integrated Chemical BioPhysics Research, Faculty of Science, Universiti Putra Malaysia, 43400 UPM Serdang, Selangor Darul Ehsan, Malaysia
[3] Laboratory of Natural Products, Institute of Bioscience, Universiti Putra Malaysia, 43400 UPM Serdang, Selangor Darul Ehsan, Malaysia

*Corresponding author: basya@upm.edu.my

Received: 1 September 2025; Revised: 12 January 2026; Accepted: 8 April 2026; Published: 28 April 2026

Abstract
Dengue virus (DENV) nonstructural protein 3 (NS3) helicase is essential for viral replication and therefore an ideal target for antiviral drug development. In this study, three compounds, epigallocatechin gallate (EGCG), ST-610 and ribavirin, were screened for inhibitory activity against DENV2 NS3 helicase using molecular docking and two independent 200 ns molecular dynamics (MD) simulations. Docking led to strong binding affinities, the highest of which was EGCG (–8.3 kcal/mol), then ST-610 (–7.8 kcal/mol) and ribavirin (–7.2 kcal/mol). MD simulations revealed structural stability in both runs throughout, with the lowest RMSD by EGCG (0.272 ± 0.019 nm) compared to ST-610 (0.345 ± 0.070 nm) and ribavirin (0.314 ± 0.031 nm). Residue flexibility analysis (RMSF) also highlighted EGCG as the most stabilizing ligand at the catalytic residues (0.130 ± 0.067 nm). Solvent accessible surface area (SASA) was highest in case of EGCG (22.20 ± 0.47 nm²) and represents good conformational flexibility, while ribavirin formed the highest number of hydrogen bonds (7.07 ± 1.17) but had lesser global stability. Together, these findings suggest that EGCG has stronger inhibitory activity through the coupling of high affinity binding and structural stabilization of catalytically important residues. The current work provides mechanistic insights into ligand-NS3 helicase interactions and recognizes EGCG as a candidate for designing dengue antiviral drugs.

Keywords: NS3 helicase, dengue virus, molecular docking, molecular dynamics simulation, antiviral drug design

Introduction

Dengue virus (DENV) infection remains the most significant mosquito-transmitted viral disease, threatening nearly half of the world population, with DENV serotype 2 (DENV2) most commonly associated with severe clinical presentations [1]. Despite more than four decades of study, no universally accepted antiviral treatment for dengue exists, highlighting the need for the identification of an effective therapeutic candidate. The DENV2 NS3 helicase is a multipurpose enzyme that is essential for viral replication, performing ATP-dependent viral RNA unwinding [2]. Additionally, the highly conserved catalytic core of NS3 helicase makes it a promising target for broad-spectrum antiviral intervention. Disruption of this enzyme by inhibition is possible and could prevent viral genome replication, thereby breaking the infectious cycle [3]. Various compounds have been found to exhibit antiviral efficacy against flaviviruses. The selection of ribavirin, EGCG and ST-610 in this study was intended to enable a mechanistic comparison among ligands with distinctly different chemical frameworks and pharmacological profiles. Ribavirin, a broad-spectrum nucleoside analogue with established efficacy, has shown broad-spectrum antiviral activity but is plagued by toxicity and heterogeneity of activity against dengue [2]. Furthermore, ribavirin is a clinically approved nucleoside analogue characterised by high polarity and limited molecular flexibility, serving as a reference compound for conventional antiviral inhibition [4, 2]. In contrast, epigallocatechin

gallate (EGCG) is a polyphenolic natural compound with high conformational flexibility and multiple hydrogen bond donor and acceptor groups, enabling diverse interaction patterns with viral proteins [5-7]The predominant catechin in green tea has recently emerged as a broad-spectrum natural antiviral with multiple molecular targets such as viral entry and enzymatic activity, making it an attractive candidate for dengue antiviral development [5].

Meanwhile, ST-610, a benzoxazole derivative, was already well defined as a highly potent flavivirus helicase inhibitor with a promising chemical scaffold for drug development and provides a structurally rigid and target-specific scaffold optimised for enzyme inhibition [8]. But a thorough comparison of these molecules with DENV2 NS3 helicase using computational methods is yet to be conducted. Comparative analysis of these ligands allows elucidation of how molecular flexibility, interaction dynamics and electronic properties contribute to different NS3 helicase inhibition mechanisms beyond previously reported antiviral potency. Computational tools such as molecular docking and molecular dynamics (MD) simulations are powerful tools that give robust information regarding drug-target interactions at the atomic level, which can be used to assess the binding affinity, structural stability and dynamic conformational rearrangement [11, 12]. Such techniques not only complement experimental results but also accelerate the identification of efficient lead molecules. In this, we performed thorough molecular docking and replicated 200 ns MD simulations to evaluate and compare the inhibitory activity of ribavirin, EGCG and ST-610 against NS3 helicase (NS3h) of DENV2. Additional calculations, including quantum chemical calculations like density functional theory (DFT) and molecular electrostatic potential (MESP), were also performed to better elucidate their electronic and structural properties relevant to protein binding. This work attempts to bring the natural compounds and synthetic compounds under one computational platform and subsequently identify potential candidates for further experimental investigations as antivirals against dengue.

Materials and Methods

Preparation of NS3 helicase DENV2

Crystal structure of dengue virus serotype 2 NS3 helicase was retrieved from the Protein Data Bank (PDB ID: 2BHR, 2.4 Å resolution) (www.rcsb.org). The structure was solved using GROMACS 2022.1. Energy minimisation was performed with 500 steps of steepest descent and 2000 steps of conjugate gradient to remove steric collisions prior to simulation [13]. The catalytic binding site was found employing diverse approaches: (i) CastP server for identifying pockets and cavities, (ii) Clustal Omega for multiple sequence alignment to detect conserved catalytic residues, (iii) PyMOL superposition of homologous helicase structures and (iv) COACH meta-server predictions of ligand binding residues [14]. The predicted binding pocket was confirmed around residues Leu189–His452, in between the two functional domains of NS3. All the protonation sites of amino acids were assigned at physiological pH (7.0).

Ligand preparation and optimisation for molecular simulations

The three molecules, ribavirin (PubChem CID: 37542), epigallocatechin gallate (EGCG; PubChem CID: 65064) and ST-610, were selected as test ligands. The 2D structures of ribavirin and EGCG were downloaded in .sdf format from PubChem, while the structure of ST-610 was manually sketched based on the published article [9]. Hydrogen atoms were added, geometries were energy-minimised and the structures were converted to 3D using Avogadro. Each of the ligands was then optimised with density functional theory (DFT) at the B3LYP/6-31G* level using Gaussian 09 to produce stable conformations. Topology and parameter files were generated using Automated Topology Builder (ATB 3.0) [15].

Molecular docking and binding interaction analysis

Molecular docking was performed to determine the binding modes of ribavirin, ST-610 and EGCG with NS3 helicase. The docking was achieved using AutoDock 4.2.6 and AutoDock Vina (2021). The grid box was centred over the catalytic cleft (x = –10.427 Å, y = 46.372 Å, z = 21.787 Å) with dimensions 70 × 68 × 72 Å to cover the active site residues. Exhaustiveness was maintained at 8, and 50 docking runs were set for every ligand. Docking poses were ranked according to binding free energy (ΔG) and visualised with Biovia Discovery Studio Visualizer 2021. Only then, all results compared to identify the analogues with lower binding energy and better conformation as the most favoured drug candidates for NS3h of DENV2.

Pharmacokinetics and toxicity prediction

Ligand pharmacokinetic properties were assessed using the SwissADME server [16], focusing on gastrointestinal (GI) absorption, blood–brain barrier permeability, drug-likeness (Lipinski's rule of five) and bioavailability scores. Toxicity profiles and predicted LD_{50} values were estimated using ProTox-II (https://tox.charite.de/protox3/) and pkCSM (https://biosig.lab.uq.edu.au/pkcsm/prediction).

Molecular dynamics simulations of the top 3 complexes

The three ligand-NS3 helicase DENV2 complexes

were subjected to molecular dynamics (MD) simulations using GROMACS 2022.1 and the GROMOS 54A7 force field. The systems were equilibrated within a TIP3P water cubic box with periodic boundary conditions and counter-ions were used to neutralise them, and then under the NVT and NPT ensembles. Energy minimisation (1000 steps steepest descent) was performed before equilibration. Simulations were performed at 200 ns in replicates for each complex at 300 K and 1 bar using the v-rescale thermostat and Berendsen barostat [17]. Trajectories were saved every 2 ps. Analysis included root-mean-square deviation (RMSD), root-mean-square fluctuation (RMSF), solvent-accessible surface area (SASA), radius of gyration (Rg) and occupancy of hydrogen bonds. The data were analysed by GROMACS and locally written codes. Meanwhile, molecular graphics images were prepared using VMD. Principal component analysis (PCA) was used to validate significant motions of the protein–ligand complexes.

Calculations by density functional theory (DFT) and molecular electrostatic potential (MESP) iso-surface Analysis

For exploring the electronic character of the ligands, frontier molecular orbital (FMO) calculations of ribavirin, ST-610 and EGCG were performed at the DFT (B3LYP/6-31G* level on Gaussian 09. The highest occupied molecular orbital (HOMO), the lowest unoccupied molecular orbital (LUMO), and the energy gap were calculated [18]. Particularly in this study, MESP can help in identifying potential binding sites for drug molecules in the NS3 helicase of DENV2. Molecular electrostatic potential (MESP) maps at the same level of theory were calculated to reveal electron-rich and electron-deficient regions, to help interpret ligand–protein interaction. Visualisation was carried out with GaussView at iso-surface cut-off values of 0.001 au.

Results and Discussion

NS3 helicase (NS3h) of DENV2 is a viral polyprotein that is essential for replication because it unwinds RNA by the mechanism of ATP hydrolysis [19]. It has three subdomains, D1 (residues 1–140) and D2 (residues 141–301) are responsible for RecA-like domains containing conserved motifs for binding ATP as well as RNA, while D3 (residues 302–451) clamps ssRNA for stability [20]. The main binding pocket selected in this study is D2-D3, with an area of 1646 Å^2 and volume of 1415 Å^3 as demonstrated in **Figure 1**. Since it contains a conserved structure and is essential for the replication of the genome, NS3h is a promising target for antiviral therapy. The active binding pocket of NS3h is situated at the interface between its domains and is defined by the catalytic triad residues His320, Asp242 and Ser435. In addition to these key residues, several other amino acids contribute to the active site, including Thr122, Ser197, Ile198, Arg220, Lys221, Asp242, Met262, Thr283, Ser285, Ser286, Asp374 and Arg432.

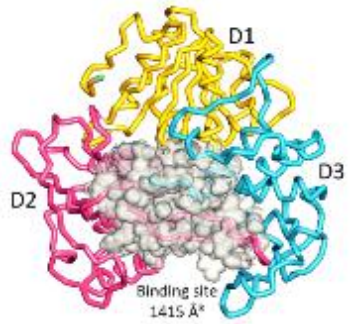

Figure 1. Three-dimensional structure of the NS3h of DENV2. The RecA-like subdomains 1 and 2 are shown in yellow and pink, respectively, domain 3 in cyan, with the binding site region highlighted by a grey shadow

Here, molecular docking was employed to predict the binding orientations and conformations of ribavirin, ST-610 and EGCG towards NS3h of DENV2. Optimised ligands were docked with AutoDock v.4.2.6 and AutoDock Vina (v.2021), and binding affinities were considered with respect to the NS3h catalytic site. Docking scores were utilised as a principal criterion to assess potential inhibitory activity. Among the three ligands, EGCG exhibited the largest binding energy (−8.3 kcal/mol), followed by that of ST-610 (−7.8 kcal/mol) and ribavirin (−7.2 kcal/mol), which signifies that both EGCG and ST-610 possess stronger inhibitory activity towards NS3h compared with that of ribavirin. The non-covalent interactions in the binding pocket were studied using BIOVIA Discovery Studio, which highlighted that ribavirin formed hydrogen bonds with Thr122, Glu245, Pro281 and Thr283, and also interacted with Thr122 and Glu245. These interactions were relatively few in number and strength and would be responsible for the reduced binding energy achieved. EGCG, on the other hand, possessed a vast interaction network with Ser197, Ile198, Arg220, Thr241, Asp242, Arg432 and Asp436 hydrogen-bonding, coupled with other interactions with Lys199, Lys221 and Leu276.

The extensive interaction profile indicates great complementarity between EGCG and the NS3h active site, raising both stability and specificity of binding. ST-610 exhibited an intermediate but positive binding profile, interacting with Lys221 and Ser435 via hydrogen bonds, together with stabilising interaction with Arg220. These serve to illustrate that ST-610 can afford to have good anchoring within the helicase

catalytic cleft and can provide stable inhibition despite a slightly reduced affinity compared to EGCG. Overall, the result classifies EGCG and ST-610 as more promising NS3h inhibitors than ribavirin, as would be anticipated through their greater docking scores and more profound interaction profiles. The binding interactions of EGCG, in particular, are in agreement with the reported ability of EGCG to block viral replication by direct protein binding, whereas ST-610 is reported as a small-molecule inhibitor of possible antiviral activity. Together, the above results justify further evaluation of EGCG and ST-610 as potential dengue therapeutics against NS3h. The entire interaction patterns of all three ligands with NS3h are listed in **Table 1**, while their docking poses are displayed in **Figure 2**.

The pharmacokinetic and toxicity profiles of ribavirin, ST-610 and EGCG were assessed using SwissADME, ProTox-II and pkCSM. All ligands satisfied Lipinski's rule of five (RO5), except EGCG, which exceeded the donor and acceptor limits, consistent with its predicted poor gastrointestinal (GI) absorption. Ribavirin exhibited the lowest molecular weight (244.21 g/mol) and high polarity, indicating good solubility but limited lipophilicity (log P = 0.13). ST-610 showed good hydrophilic–lipophilic balance (log P = 2.25) and TPSA within the optimal range (117.97 Å²), indicating favourable absorption. Ribavirin (143.72 Å²) was on the borderline, while EGCG (197.37 Å²) was above, indicating lower absorption potential. Toxicity prediction placed ribavirin and ST-610 in Class 5 (LD50 ≈ 5000 mg/kg), suggesting a general safety margin, whereas EGCG was in Class 3 (LD50 ≈ 2000 mg/kg), suggesting a higher risk. All the ligands were endowed with a general bioavailability score (0.55), implying drug-likeness of moderate grade. Overall, ST-610 exhibited the best ADMET profile with high GI absorption, low toxicity and RO5 compliance. The ADMET properties of curcumin and its analogues are listed in **Table 2**, offering further insights into their drug-likeness and overall suitability for therapeutic applications.

Table 1. Molecular docking interpretation of ribavirin, ST-610 and EGCG against the NS3h of DENV2, highlighting their binding affinities and interaction profiles

Ligands	Binding affinity (kcal/mol)	H-Bond Residues	No. of H-Bonds	Other Bond Residues	Structures
ST-610	–7.8	Lys221 Ser435	2	Arg220	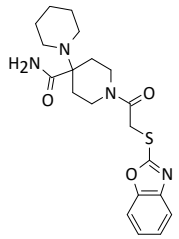
Ribavirin	−7.2	Thr122 Glu245 Pro281 Thr283	4	Thr122 Glu245	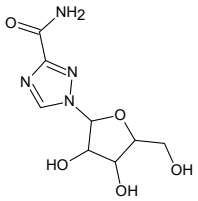
EGCG	−8.3	Ser197 Ile198 Arg220 Thr241 Asp242 Arg432 Asp436	7	Lys199 Lys221 Leu276	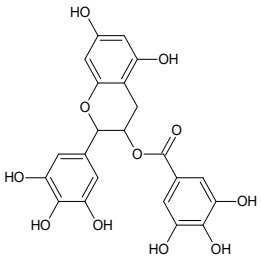

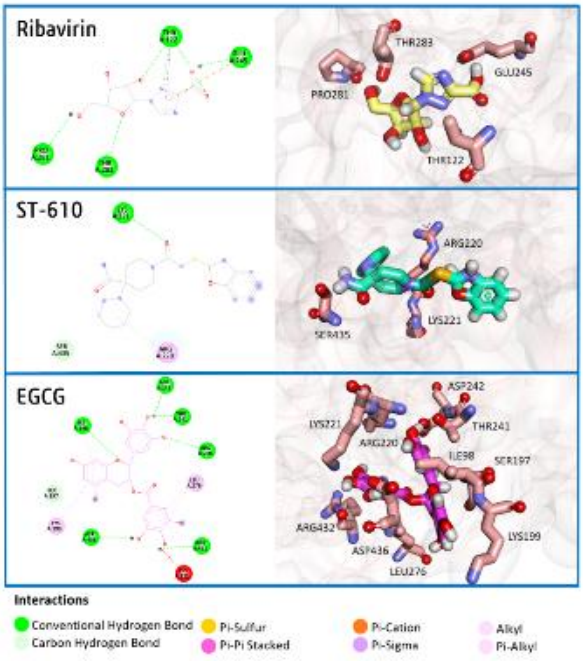

Figure 2. Docking poses illustrating the predicted spatial arrangements and hydrogen bond interactions of ribavirin, ST-610 and EGCG within the binding site of NS3h of DENV2

Table 2. Toxicity profiles of ribavirin, ST-610 and EGCG with their drug parameters

Ligands	M/W (g/mol)	Number of Rotatable Bonds	Number of H-bond Acceptors	Number of H-bond Donors	Log $P_{o/w}$	Log S	TPSA (Å^2)	Toxicity (mg/kg)
ST-610	402.51	6	5	1	2.25	-3.63	117.97	LD50: 5000 Class: 5
Ribavirin	244.21	3	8	4	0.13	-0.21	143.72	LD50: 5000 Class: 5
EGCG	458.37	4	11	8	1.87	-3.56	197.37	LD50: 2000 Class: 3

The MD simulations provided valuable insights into the stability and conformational behaviour of the NS3 helicase-ligand complexes for ribavirin, ST-610 and EGCG. All three drug-protein complexes demonstrated good structural stability throughout the simulation as per the root mean square deviations (RMSDs) as depicted in **Figure 3(A)**. EGCG had the lowest RMSD value of 0.272 ± 0.020 nm, reflecting a highly stable interaction with very little variation from the starting structure. Ribavirin was the next with 0.314 ± 0.031 nm, also reflecting good stability. ST-610 possessed a slightly larger RMSD (0.345 ± 0.070 nm) but within a satisfactory range of stability, which might suggest that its bulkier scaffold is accountable for more conformationally flexible binding modes. Meanwhile, root mean square fluctuation (RMSF) analysis (**Figure 3(B)**) revealed that the catalytic triad residues of NS3 helicase were less than 0.15 nm in all cases, demonstrating well-conserved protein–ligand contacts. EGCG (0.130 ± 0.067 nm) and ribavirin (0.132 ± 0.075 nm) indicated somewhat more restricted motion, while ST-610 (0.156 ± 0.093 nm) provided reasonable flexibility, which could reflect its atypical binding orientation and lipophilic interactions. Fluctuations were mostly limited at residues 8, 83, 300 and 356, which are the loop areas that are recognised to be more flexible. Interestingly, the flexible areas were not at the catalytic pocket and the resulting functional stability of the enzyme upon ligand binding.

Moreover, the radius of gyration (R_g) of ribavirin

exhibited a compact complex structure with R_g = 0.223 ± 0.001 nm, which showed that its smaller nucleoside-like shape was well fit into the helicase binding site. ST-610 had an R_g of 0.226 ± 0.002 nm, indicating a compact but stable protein–ligand complex, consistent with its bulkier aromatic nature that may induce minor conformational adjustments. EGCG had an R_g of 0.225 ± 0.002 nm, demonstrating that despite its presence of a polyphenolic backbone with numerous hydroxyl moieties, the complex remained compact and structurally uniform (**Figure 3(C)**). Furthermore, solvent accessible surface area (SASA) measurements revealed the surface exposure upon ligand binding as portrayed in **Figure 3(D)**. Ribavirin possessed 22.00 ± 0.47 nm², which represented effective burial within the binding site with minimal solvent exposure. ST-610 possessed 22.04 ± 0.59 nm², which reflected stable solvent interactions corresponding to its bulkier structure. EGCG, with 22.20 ± 0.47 nm², showed slightly greater exposure, which could be due to its hydrophilic hydroxyl groups dynamically interacting with the solvent environment while retaining overall stability.

Next, the mean distance of NS3h to the ligands was consistent with stable binding, with close contacts of ribavirin (0.142 ± 0.007 nm) and EGCG (0.158 ± 0.010 nm), while ST-610 (0.229 ± 0.022 nm) had a little wider range of contact due to its bulk structure (**Figure 3(E)**). Hydrogen bond analysis also revealed varying interaction profiles, as shown in **Figure 3(F)**. Ribavirin contained the highest number of hydrogen bonds (7.07 ± 1.17), consistent with its polar functional groups. The molecule possesses multiple hydroxyl (–OH) groups on the ribose moiety, an amide (–C(=O)–NH–) group and a primary amine (–NH_2), all of which provide numerous donor and acceptor sites for hydrogen bonding. These polar functional groups enhance its ability to form stable interactions with residues within the NS3h binding pocket. While EGCG also participated in strong hydrogen bonding (4.58 ± 1.32), with its multiple hydroxyl substituents. ST-610, having fewer hydrogen bonds (0.68 ± 0.67), might be able to rely more on hydrophobic and π–π interactions, which play significant roles in drug–protein complex stabilisation as well. Thus, while ribavirin demonstrates the most consistent polar-driven interaction profile, EGCG and ST-610 exhibit complementary stabilisation mechanisms through hydrogen bonding flexibility and hydrophobic or aromatic interactions, respectively, highlighting mechanistically distinct inhibition strategies rather than a single dominant binding mode.

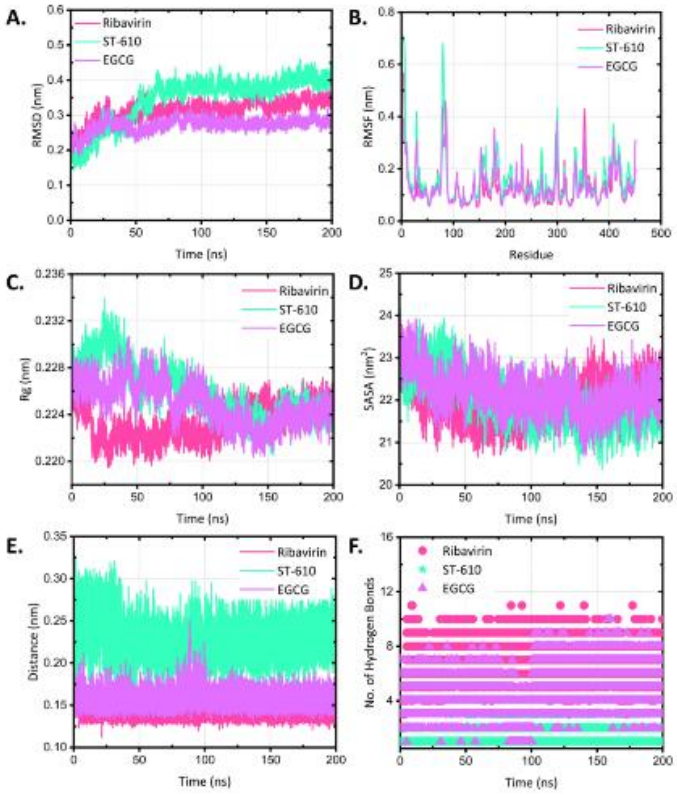

Figure 3. The average of triplicate molecular dynamics simulation for ribavirin, ST-610 and EGCG against NS3h of DENV2 after 200ns (A) RMSD (B) RMSF (C) Radius of gyration (D) SASA (E) Distance (F) Number of hydrogen bonds

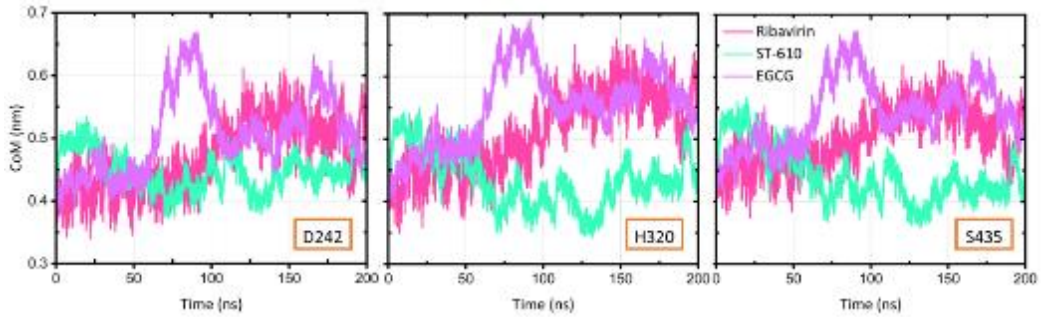

Figure 4. The CoM distance between ribavirin, ST-610 and EGCG against the catalytic triads of NS3h of DENV2 (Ser435, Asp242, His320)

To further analyse the binding mode of the ligands with NS3h, centre of mass (CoM) distances between each of the ligands and catalytic triad residues (D242, H320 and S435) were calculated during the period of the simulation (**Figure 4**). The calculated average CoM distances confirmed that for S435, ribavirin was maintained at a distance of 0.501 ± 0.047 nm, ST-610 at 0.443 ± 0.043 nm and EGCG at 0.540 ± 0.053 nm. For H320, the corresponding values were 0.511 ± 0.063 nm (ribavirin), 0.435 ± 0.043 nm (ST-610) and 0.550 ± 0.061 nm (EGCG). Similarly, for D242, ribavirin was 0.471 ± 0.054 nm, ST-610 was 0.447 ± 0.029 nm, and EGCG was 0.506 ± 0.064 nm.

Interestingly enough, these CoM findings do not necessarily match the results of the average ligand-protein distance study, in which ribavirin exhibited tighter average distances to the catalytic residues. This divergence between atomistic distance metrics and CoM analysis highlights the importance of integrating multiple structural descriptors to capture ligand-specific binding mechanisms, which cannot be inferred from binding proximity alone. The reason could be that the values of average distances measure specific atom-to-atom contacts, while CoM analysis examines the general ligand mass distribution in relation to the catalytic triad [21]. Thus, while ribavirin will form direct hydrogen bonding interactions with the catalytic residues, ST-610 is in a more compact overall position compared to the active site, as reflected by its smaller CoM values. EGCG, however, despite forming numerous hydrogen bonds and solvent contacts, had slightly greater CoM distances at which were most likely due to its bulky polyphenolic structure extending deeper into the binding pocket. Overall, the CoM analysis suggests that ST-610 consistently has the most constricted binding pose in close vicinity to the catalytic triad, whereas ribavirin attains stability through strong direct interactions and EGCG stabilises through an extended binding mode. This indicates that the ligands adopt distinct but complementary binding modes to target NS3h of DENV2.

The close contact and interaction analysis revealed distinct binding patterns of ribavirin, ST610 and EGCG to the DENV2 NS3h. Ribavirin formed hydrogen bonds with Lys263, Thr122, Glu245, Cys318, Asp315 and His320, apart from other non-covalent contacts with Cys261. Among them, His320 is a residue of the catalytic triad, and it implies that ribavirin has the ability to fit into the active site but with very limited interaction with the entire catalytic network. ST-610, on the other hand, formed a single hydrogen bond with Glu323 and also a non-hydrogen bonding interaction with Lys221, Arg432, Pro124, Ala125, Cys261 and Leu276. Although ST-610 forms interaction with several residues around the catalytic cavity, its lack of stable hydrogen bonding with the catalytic triad may result in lower inhibitory activity compared to the other ligands [22]. Lastly, EGCG possessed the largest network of interaction, forming hydrogen bonds with Thr241, Asp242, Arg220, Asp436, Ala431, Ser435 and Ser197, and secondary contacts with residues such as Ile198, Leu276, Met262, Ile243, Pro264, Ala439, Pro376 and Arg432. EGCG uniquely interacted directly with two catalytic residues (Asp242 and Ser435) established to be essential for helicase function. The location of the catalytic residues can be seen in **Figure 5**.

These findings are consistent with previous reports that curcuminoids and polyphenolic analogues inhibit NS3h through a synergy of aromatic stacking, hydrophobic contacts and electrostatic interactions in which the aromatic forces are significant [2, 5]. Significantly, while a number of aromatic residues in NS3h are concealed in the binding pocket, the surface of the outer helicase is charged and contains acidic and basic residues, offering avenues for electrostatic and hydrogen-bonding interactions [23]. Collectively, interaction and structural analyses reveal that all three ligands form stable complexes with distinct mechanistic behaviours of NS3h. EGCG exhibits an

optimal binding profile, achieving stability through adaptive hydrogen-bond networks that engage the catalytic triad residues and neighbouring amino acids, allowing conformational accommodation within the binding pocket. Ribavirin, in contrast, relies on compact, polar-driven interactions with limited flexibility, primarily engaging part of the catalytic site. ST-610 maintains a rigid binding pose with minor conformational fluctuations, consistent with its bulky aromatic scaffold and interacts peripherally around the active site. These results suggest that ligand stability and inhibitory potential are governed not only by binding strength but also by differences in flexibility, compactness, solvent exposure and specific interaction patterns. Taken together, these findings highlight the mechanistic diversity of NS3h inhibition among EGCG, ribavirin and ST-610, with EGCG demonstrating the most adaptable and extensive engagement, supporting its consideration for further optimisation as a potential inhibitor.

PCA was employed to characterise the concerted motions of NS3h in its complex with ribavirin, ST-610 and EGCG as depicted in **Figure 6**. Arrows represent the dominant direction of motion, and the red and blue traces denote the initial and final conformations, respectively [3]. For the ribavirin complex, the protein underwent limited conformational change with arrows mostly in flexible loop regions. This shows ribavirin binding preserved the general structural core while allowing periphery motions, consistent with its stabilising hydrogen-bond interactions. Meanwhile, the ST-610 complex had relatively limited motions, as suggested by fewer large direction arrows. This finding is in agreement with the tight binding mode suggested by CoM distance analysis, suggesting that ST-610 inhibits large-scale domain rearrangement and stabilises helicase conformation.

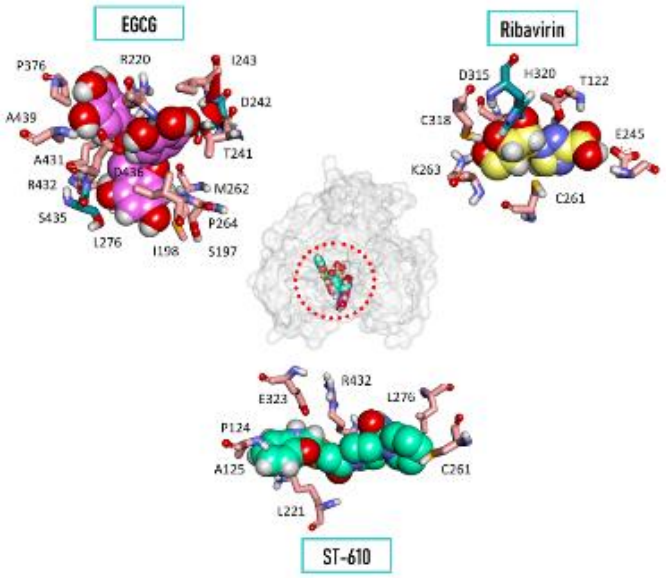

Figure 5. Snapshots illustrate the binding orientation of ribavirin, ST-610 and EGCG within the active site of NS3h at their closest approach. The catalytic triad is represented in green liquorice, whereas other key residues of the binding pocket are displayed in pink

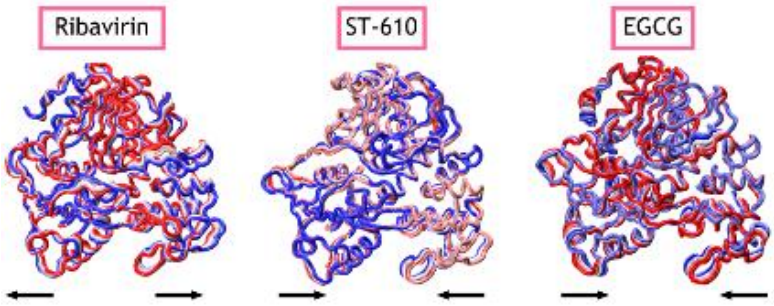

Figure 6. The structures illustrate the dynamic motions of NS3h DENV2 with ribavirin, ST-610 and EGCG as revealed by PCA. The arrows denote the direction of the movement, with the red trace showing an initial conformation and the blue displaying the final orientation

On the other hand, more localised motions in various regions were observed for the EGCG complex, as would be expected for the bulky polyphenolic molecule EGCG crossing several subdomains. Although it introduced a somewhat larger conformational change, the protein structurally remained unperturbed, indicating that EGCG maintains the enzyme through numerous hydrogen bonds and solvent contacts but nonetheless permits flexibility of the domains. In conclusion, PCA indicates that the three ligands stabilise NS3h but by distinct mechanisms, at which ribavirin preserves hydrogen-bond-catalyzed stability, ST-610 constrains motion by closely placed restriction, and EGCG facilitates support of stability and provokes more extensive flexibility. This heterogeneity of binding-induced dynamics can be useful in drug design because each ligand highlights distinct modes of inhibition of NS3h of DENV2. These interaction patterns reveal three distinct inhibitory behaviors, ribavirin primarily stabilises NS3h through direct polar contacts with catalytic residues, ST-610 adopts a compact, catalytically peripheral binding pose dominated by hydrophobic interactions, and EGCG uniquely bridges multiple catalytic and surrounding residues through an extended hydrogen-bonding network.

To understand the binding affinity profiles of the selected ligands with NS3h of DENV2 in a deeper manner, density functional theory (DFT) and molecular electrostatic potential (MESP) iso-surface computations were carried out, as demonstrated in **Figure 7** [24, 25]. These computations provide data regarding the distribution of electrons as well as potential binding sites of the molecules. Ribavirin, with its multiple polar functional groups, exhibited an equilibrated electrostatic potential that supports stable hydrogen bonding with catalytic residues. EGCG, possessing intense hydroxyl substituents, registered the lowest minimum negative potential (Vmin), consistent with its extensive hydrogen bonding and solvent-accessible interactions. ST-610, in contrast, registered the highest Vmin, reflecting its preference for hydrophobic and aromatic stacking interactions over extensive hydrogen bonding. Overall, Vmin trend (EGCG < ribavirin < ST-610) is in line with the corresponding modes of interaction determined from molecular docking and MD simulations, pointing out that all ligands stabilise NS3h by virtue of complementary electrostatic and structural moieties.

Electronic properties of ribavirin, ST-610 and EGCG are associated with their pharmacological action and are also pertinent to the study of molecular interaction governing drug–target binding. DFT calculations were done to investigate the electronic properties and energy gap of the compounds, which are important for estimation of stability, reactivity and their potential binding efficiency with NS3h [26]. ST-610 possessed the largest HOMO–LUMO gap (7.4287 eV), which was followed by EGCG (7.1838 eV), with the lowest gap found for ribavirin (5.4777 eV). The larger the HOMO–LUMO gap, the more electronic stability and lower chemical reactivity it indicates, suggesting that ST-610 is relatively more stable than EGCG and ribavirin. The calculated HOMO and LUMO energy values are presented in **Table 4**.

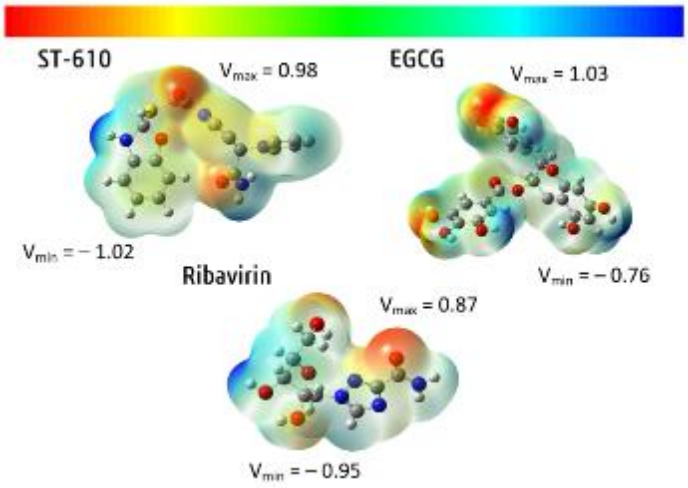

Figure 7. MESP iso-surface analysis of ribavirin, ST-610 and EGCG highlights regions of electrostatic potential critical for binding interactions. Red regions denote negative potential, blue indicates positive potential and green represents neutral areas

Table 4. HOMO-LUMO energy gap serves as a valuable parameter for estimating the stability and reactivity of ligand molecules, providing insights that are essential for rational drug design

Ligands	HOMO (eH)	LUMO (eH)	HOMO-LUMO (eV)
ST-610	– 0.2940	– 0.0210	7.4287
Ribavirin	– 0.2451	– 0.0438	5.4777
EGCG	– 0.3041	– 0.0401	7.1838

Table 5. Comparative analysis of NS3 helicase-ligand complexes

Ligand	RMSD (nm)	RMSF (nm)	H-bonds	HOMO–LUMO (eV)	MESP Vmin (kcal/mol)	Mechanistic Insight
Ribavirin	0.314 ± 0.031	0.132 ± 0.075	7.07 ± 1.17	5.478	Moderate	Polar-driven binding, strong direct H-bonds with catalytic residues, limited flexibility
ST-610	0.345 ± 0.070	0.156 ± 0.093	0.68 ± 0.67	7.429	Highest	Peripheral binding relies on hydrophobic and π–π interactions, minor conformational adjustments
EGCG	0.272 ± 0.020	0.130 ± 0.067	4.58 ± 1.32	7.184	Lowest	Extended binding, engages catalytic triad and neighbouring residues, flexible H-bond network, high solvent adaptability

Conversely, the lower energy gap of ribavirin has greater chemical reactivity with simpler electronic transitions that may enhance its capacity for interaction with the target protein. The interpretation of the MESP iso-surface provides insight into the distribution of the electrostatic potential of these ligands. The red regions show negative electrostatic potential, the blue regions show positive potential, and the green regions of neutral potential. These charge distributions are relevant to predict hydrogen bonding and electrostatic interactions in the NS3 helicase active site. Relevantly, ST-610 and EGCG exhibit large areas of negative potential, which may allow for stronger electrostatic complementarity with positively charged amino acids, while ribavirin exhibits more localised charge distribution. Cumulatively, the combined DFT and MESP analysis suggests that ST-610, having its larger HOMO–LUMO gap and superior charge distribution, is potentially more stable and binding-specific for NS3 helicase. EGCG is also demonstrating good interaction capacity and stability, whereas ribavirin, although more reactive, may use its higher reactivity to form stronger transient interactions. Comparative metrics for RMSD, RMSF, hydrogen bonds, HOMO–LUMO gaps, and MESP potentials are summarised in **Table 5**, highlighting distinct mechanistic inhibition among the ligands.

These findings confirm the molecular docking and MD simulation results in favour of EGCG and ribavirin as superior candidates over ST-610. The agreement between electrostatic potential distribution, HOMO–LUMO gaps and MD-derived interaction profiles demonstrates that electronic properties directly influence ligand binding behaviour, with EGCG favouring electrostatic adaptability, ribavirin promoting reactive polar engagement and ST-610 exhibiting electronically stable but less reactive binding.

Conclusion

In silico screening of NS3h of DENV2 with ribavirin, ST610 and EGCG reveals distinct inhibition potentials. EGCG consistently presented the best features, including stable and ongoing interactions with the key catalytic residues and low RMSD values, thereby demonstrating its great potential as a natural NS3 helicase inhibitor. Ribavirin showed good consistency of pattern of interaction and remains significant in view of its broad-spectrum antiviral activity and potential complementary effect in helicase inhibition. Conversely, ST610 provided valuable mechanistic information in the form of centre of mass and MESP analyses that revealed unique electrostatic characteristics that may determine the way it orients while binding, although its overall stability and interaction profile were less appealing compared to those of ribavirin and EGCG.

Cumulatively, these findings position EGCG and ribavirin as the more promising candidates for inhibition against NS3 helicase, with ST610 as a second lead that requires optimisation to enhance its modest but distinctive interaction profile.

Acknowledgement

The authors acknowledge the Institute for Medical Research (Dr. Ami Fazlin Syed Mohamed), Ministry of Health, Malaysia, and the Geran Putra Inisiatif (GPI9777100, Universiti Putra Malaysia, for providing the facilities and support to carry out this research.

References

1. Phadungsombat, J., Nakayama, E. E., & Shioda, T. (2024). Unraveling dengue virus diversity in Asia: An epidemiological study through genetic sequences and phylogenetic analysis. *Viruses,* 16(7), 46.
2. Dharmapalan, B. T., Biswas, R., Sankaran, S., Venkidasamy, B., Thiruvengadam, M., George, G., Rebezov, M., Zengin, G., Gallo, M., Montesano, D., Naviglio, D., & Shariati, M. A. (2022). Inhibitory potential of chromene derivatives on structural and non-structural proteins of dengue virus. *Viruses,* 14(12), 2656.
3. Sarto, C., Kaufman, S. B., Estrin, D. A., & Arrar, M. (2020). Nucleotide-dependent dynamics of the dengue NS3 helicase. *Biochimica et Biophysica Acta (BBA) - Proteins and Proteomics, 1868*(8), 140441.
4. Chahal, V., Nirwan, S., Pathak, M., & Kakkar, R. (2022). Identification of potent human carbonic anhydrase IX inhibitors: A combination of pharmacophore modeling, 3D-QSAR, virtual screening and molecular dynamics simulations. *Journal of Biomolecular Structure and Dynamics,* 40(10), 4516–4531.
5. Loaiza-Cano, V., Monsalve-Escudero, L. M., Filho, C., Martinez-Gutierrez, M., & Sousa, D. P. (2020). Antiviral role of phenolic compounds against dengue virus: A review. *Biomolecules,* 11(1), 11.
6. Sarowska, J., Wojnicz, D., Jama-Kmiecik, A., Frej-Madrzak, M., & Choroszy-Krol, I. (2021). Antiviral potential of plants against noroviruses. *Molecules,* 26(15), 4669.
7. Siraj, A., Naqash, F., Shah, M. A., Fayaz, S., Majid, D., & Dar, B. N. (2021). Nanoemulsions: Formation, stability and an account of dietary polyphenol encapsulation. *International Journal of Food Science & Technology,* 56(9), 4193–4205.
8. Norazharuddin, H., & Lai, N. S. (2018). Roles and prospects of dengue virus non-structural proteins as antiviral targets: An easy digest. *Malaysian Journal of Medical Sciences,* 25(5), 6–15.
9. Byrd, C. M., Grosenbach, D. W., Berhanu, A., Dai, D., Jones, K. F., Cardwell, K. B., Schneider, C., Yang, G., Tyavanagimatt, S., Harver, C., Wineinger, K. A., Page, J., Stavale, E., Stone, M. A., Fuller, K. P., Lovejoy, C., Leeds, J. M., Hruby, D. E., & Jordan, R. (2013). Novel benzoxazole inhibitor of dengue virus replication that targets the NS3 helicase. *Antimicrobial Agents and Chemotherapy,* 57(4), 1902–1912.
10. Sweeney, N. L., Hanson, A. M., Mukherjee, S., Ndjomou, J., Geiss, B. J., Steel, J. J., Frankowski, K. J., Li, K., Schoenen, F. J., & Frick, D. N. (2015). Benzothiazole and pyrrolone flavivirus inhibitors targeting the viral helicase. *ACS Infectious Diseases,* 1(3), 140–148.
11. Rafi, M. O., Bhattacharje, G., Al-Khafaji, K., Taskin-Tok, T., Alfasane, M. A., Das, A. K., Parvez, M. A. K., & Rahman, M. S. (2022). Combination of QSAR, molecular docking, molecular dynamic simulation and MM-PBSA: Analogues of lopinavir and favipiravir as potential drug candidates against COVID-19. *Journal of Biomolecular Structure and Dynamics,* 40(8), 3711–3730.
12. Umar, A. K., Zothantluanga, J. H., Aswin, K., Maulana, S., Sulaiman Zubair, M., Lalhlenmawia, H., Rudrapal, M., & Chetia, D. (2022). Antiviral phytocompounds “ellagic acid” and “(+)-sesamin” of *Bridelia retusa* identified as potential inhibitors of SARS-CoV-2 3CLpro using extensive molecular docking, molecular dynamics simulation studies, binding free energy calculations, and bioactivity prediction. *Structural Chemistry,* 33(5), 1445–1465.
13. Feng, T., Hu, Z., Wang, K., Zhu, X., Chen, D., Zhuang, H., Yao, L., Song, S., Wang, H., & Sun, M. (2020). Emulsion-based delivery systems for curcumin: Encapsulation and interaction mechanism between debranched starch and curcumin. *International Journal of Biological Macromolecules,* 161, 746–754.
14. Li, S., Duan, S., Zha, Z., Pan, J., Sun, L., Liu, M., Deng, K., Xu, X., & Qiu, X. (2020). Structural phase transitions of molecular self-assembly driven by nonbonded metal adatoms. *ACS Nano,* 14(5), 6331–6338.
15. Ibezim, A., Madukaife, M. S., Osigwe, S. C., Engel, N., Karuppasamy, R., & Ntie-Kang, F. (2022). Fragment-based virtual screening discovers potential new *Plasmodium* PI4KIIIβ ligands. *BMC Chemistry,* 16(1), 19.
16. Olaokun, O. O., & Zubair, M. S. (2023). Antidiabetic activity, molecular docking, and ADMET properties of compounds isolated from bioactive ethyl acetate fraction of *Ficus lutea*

leaf extract. *Molecules, 28*(23), 7377.

17. Dey, D., Hossain, R., Biswas, P., Paul, P., Islam, M. A., Ema, T. I., Gain, B. K., Hasan, M. M., Bibi, S., Islam, M. T., Rahman, M. A., & Kim, B. (2023). Amentoflavone derivatives significantly act towards the main protease (3CLpro/Mpro) of SARS-CoV-2: In silico ADMET profiling, molecular docking, molecular dynamics simulation, network pharmacology. *Molecular Diversity,* 27(2), 857–871.
18. Huang, Y., Rong, C., Zhang, R., & Liu, S. (2017). Evaluating frontier orbital energy and HOMO/LUMO gap with descriptors from density functional reactivity theory. *Journal of Molecular Modeling,* 23(1), 3.
19. Amrein, F., Sarto, C., Cababie, L. A., Gonzalez Flecha, F. L., Kaufman, S. B., & Arrar, M. (2023). Impact of bound ssRNA length on allostery in the dengue virus NS3 helicase. *Nucleic Acids Research,* 51(20), 11213–11224.
20. Frick, D. N. (2003). Helicases as antiviral drug targets. *Drug News & Perspectives,* 16(6), 355–362.
21. Abraham, M., Alekseenko, A., Andrews, B., Basov, V., Bauer, P., Bird, H., Briand, E., Brown, A., Doijade, M., Fiorin, G., Fleischmann, S., Gorelov, S., Gouaillardet, G., Gray, A., Irrgang, M. E., Jalalypour, F., Johansson, P., Kutzner, C., Łazarski, G., & Lindahl, E. (2025). *GROMACS 2025.0 manual* (Version 2025.0). Zenodo.
22. Hasan, A. H., Murugesan, S., Amran, S. I., Chander, S., Alanazi, M. M., Hadda, T. B., Shakya, S., Pratama, M. R. F., Das, B., Biswas, S., & Jamalis, J. (2022). Novel thiophene chalcones-coumarin as acetylcholinesterase inhibitors: Design, synthesis, biological evaluation, molecular docking, ADMET prediction and molecular dynamics simulation. *Bioorganic Chemistry,* 119, 105572.
23. Kwong, A. D., Rao, B. G., & Jeang, K. T. (2005). Viral and cellular RNA helicases as antiviral targets. *Nature Reviews Drug Discovery,* 4(10), 845–853.
24. Marimuthu, R., Rameshkumar, P., Indu, S., Rajarajan, A., Saeedah, M. H., Dina, S. R., Rabab, A. N., & Arunagirinathan, A. (2023). Malacitanolide, reissantin E and paclitaxel compounds as inhibitors of envelope, NS5 and NS2B/NS3 target proteins of dengue virus: Computational docking and molecular dynamics simulations studies. *Journal of King Saud University - Science,* 35(8), 102868.
25. Wakchaure, P. D., Ghosh, S., & Ganguly, B. (2020). Revealing the inhibition mechanism of RNA-dependent RNA polymerase (RdRp) of SARS-CoV-2 by remdesivir and nucleotide analogues: A molecular dynamics simulation study. *The Journal of Physical Chemistry B,* 124(47), 10641–10652.
26. Morawietz, T., & Artrith, N. (2021). Machine learning-accelerated quantum mechanics-based atomistic simulations for industrial applications. *Journal of Computer-Aided Molecular Design,* 35(4): 557–586.